Proceedings of the 2010 3rd IEEE RAS & EMBS
International Conference on Biomedical Robotics and Biomechatronics,
The University of Tokyo, Tokyo, Japan, September 26-29, 2010

Modeling and Stability Analysis of Human Normal Walking with Implications for the Evolution of the Foot

Qining Wang, Kunlin Wei, Long Wang and Dongjiao Lv

Abstract— **This paper formulates the mathematical model of a biped that is capable of dynamic walking gaits. The model consists of hip actuation, segmented legs, flat feet and torsional spring based passive ankle stiffness. Using numerical simulations on the proposed model, we find that from the view of stability, there is optimal foot-ankle ratio of the flat-foot bipeds. The results indicate that the human foot proportion is indeed better optimized for dynamic bipedal walking than that of apes, further suggesting the current state of human foot is to some extent the product of positive selection for more stable bipedal locomotion during the evolution of the foot.**

I. Introduction

Biological studies reported that the foot proportion (the ratio from the power arm to the load arm of the foot), differs markedly in humans and apes, e.g. approximately 40% in humans, 46% in gorillas, 28.2% in chimpanzees, 19.6% in orangutans [1], [2]. As the body proportions of hominids may be functionally evolved, recent biomechanical analysis of the human foot suggest that the structure of the human foot should be expected to show mechanical benefits for bipedal standing, considering that apes' locomotion and posture are predominantly quadrupedal [3].

Human beings can achieve stable and efficient dynamic bipedal walking on various different terrains without much effort. Though people's usual gaits tend to be natural and simple, the theoretical analysis and engineering applications are complicated based on the remarkable fact that the walking motion is a complex dynamic phenomenon. Bipedal walking involves highly non-linear and multi-variable dynamics with discrete events (e.g. heel-strike, toe-strike) and a varying configuration (alternating stance and swing phases).

Different from the trajectory-based whole body models, the idea of a biped walking without joint actuation during certain phases of locomotion has been proposed [11]. The authors termed this type walk as "Ballistic Walking". Subsequently, the concept of "Passive Dynamic Walking" has been presented, which has been developed as a possible explanation for the efficiency of the human gait [10]. Such mechanism with two rigid legs can be constructed so as to descend a gentle slope with no actuation and no active control and shows a remarkable resemblance to the human gait. The mechanical energy consumption of such a mechanism may be compensated by two kinds of actuation in the case of level ground walking: apply an impulsive push along the trailing leg or apply a hip torque against the stance leg. Starting from the initial idea of "Passive Dynamic Walking", several studies investigated nonlinear dynamics of a two-link biped robot which consist of two rigid legs connected by a frictionless hinge at the hip, with point masses representing the upper body and two legs [5], [6], [8]. Based on the simplest walking model [6], a three-link passive dynamic walking model with upper body has been proposed [16]. [4] analyzed the dynamics of a five-link robot with knees and upper body. However, in these models, the bipeds are often modeled with point feet or round feet which are far from real human feet and have clear disadvantages of being unable to achieve the start and stop of walking.

In this study, we present a passivity-based bipedal model, which includes segmented legs, flat feet and linear torsional springs based ankle stiffness. Similar to previous level-ground walking models, we add a hip torque between the swing leg and the stance leg to compensate the mechanical energy consumption of the walker. We use numerical simulations to study the walking dynamics of the biped and investigate the effects of foot geometric parameters. The results can be used to explore further understanding of the evolution of the foot, and help the design of future intelligent ankle-foot prosthesis.

The rest of this paper is organized as follows. Section II describes the dynamic model and the method for stability analysis. Section III shows the simulation results. Section IV discusses the implications for the evolution of human foot.

II. Methods

A. Model

The model in this study consists of a point mass representing the upper body, two legs with knee joints and ankle joints, and two mass-added flat feet (see Fig. 1). The mass of each leg is simplified as point masses added on the Center of Mass (CoM) of the shank and the thigh respectively. The ankles are modeled as passive joints constrained by linear torsional springs. The knee will lock the shank when the shank and the thigh keep in a straight line. Relevant parameters are shown in Table I. Here, the two-dimensional model has some assumptions: 1) Shanks and thighs suffer no flexible deformation during locomotion. 2) There is no damping or friction on the hip joint. 3) Flat feet do not deform or slip during locomotion, even on uneven terrain. 4) Heel-strike and toe-strike are modeled as an instantaneous, fully inelastic impact where no slip and no bounce occurs.

This work was supported by the 985 Project of Peking University (No. 3J0865600).

Q. Wang and L. Wang are with the College of Engineering, Peking University, China. K. Wei is with the Department of Psychology, Peking University, China. D. Lv is with the Department of Biomedical Engineering, Peking University, China.

Email: Q. Wang (qiningwang@pku.edu.cn)

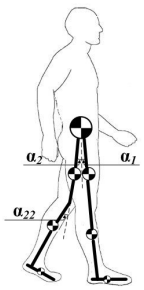

Fig. 1. Dynamic model of bipedal walking with upper body, flat feet and ankle stiffness. The global coordinates of the hip joint is notated as (x_h, y_h). α_1 and α_2 are the angles between each thigh and the vertical axis in sagittal plane respectively. The x-axis is along the level ground while the y-axis is vertical to the ground upwards.

TABLE I

MAIN PARAMETERS USED IN THE DYNAMIC WALKING MODEL AND THE FOLLOWING SIMULATIONS

Parameter	Description	Parameter	Description
m_1, m_2	leg mass	l_1, l_2	leg length
m_3	hip mass	l_{11}, l_{22}	shank length
m_{1t}, m_{2t}	thigh mass	l_{f1}, l_{f2}	foot length
m_{1s}, m_{2s}	shank mass	k	ankle stiffness
m_{f1}, m_{f2}	foot mass	P	hip torque

Recent study reported that the flat foot shape can be defined by two non-dimensional parameters: foot length and foot ratio, where the foot ratio is the ratio of the distance between the heel and ankle, to the distance from heel to toe [9]. However, there is another definition of foot ratio with implications for the evolution of the foot [3]. The ratio of the power arm of the foot to the load arm differs in humans and apes [1]. To obtain better understanding of human walking, in this study, we defined the flat foot shape by the following two parameters: l_f = (distance from heel to toe), r = (distance from heel to ankle / distance from ankle to toe). In the human foot, the toe is connected to the metatarsal by flexible joints. However, in this study, the foot is modeled as a rigid bar. Thus, we ignored the toe length and used the lever length of the foot (the distance from the heel to the distal head of the third metatarsal) as l_f. Such definition has been used in several biomechanics studies [1], [3].

The biped travels forward on level ground. The stance leg keeps contact with the ground while the swing leg pivots about the constraint hip. When the flat foot strikes the ground, there are two impulses, "heel-strike" and "toe-strike", representative of the initial impact of the heel and the following impact as the whole foot contact the ground. Note that actually when the shank swings (α_{11} or α_{22} varies), the moment of inertia of the leg changes. However, since the swing angle of the shank is relatively small and the time duration of large swing angle is quite short, we simplified the moment of inertia of the leg as a constant. Additionally, the torsional spring on each ankle constrains the foot vertical to the shank when no heel-strike or toe-strike has occurred.

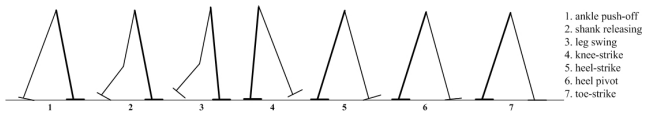

Fig. 2. The walking phases during one step sequence. The thick line represents leg 1, while the thin line represents leg 2.

B. Walking dynamics

We described one walking step with specification of seven phases (see Fig. 2). The model can be defined by the rectangular coordinates x which can be described by the x-coordinates and y-coordinates of the mass points and the corresponding angles. The walker can also be described by the generalized coordinates q. Note that in different walking phases, the specific components of x and q may be different.

1) Ankle push-off: Suppose that leg 1 (l_1) is the stance leg, while leg 2 (l_2) is the swing leg. In this phase (see Phase 1 in Fig. 2), the foot of leg 2 rotates around the ankle joint. The stance leg maintains foot contact with ground and the swing leg maintains toe contact with ground. Since the knee is locked, the walker can be described by the rectangular coordinates x and the generalized coordinates q as follows:

$$\begin{aligned} x &= [x_{m1}\ y_{m1}\ \alpha_1\ x_{m2}\ y_{m2}\ \alpha_2\ x_{m3}\ y_{m3}]^T \\ q &= \begin{bmatrix} x_h & y_h & \alpha_1 & \alpha_2 \end{bmatrix}^T \end{aligned} \quad (1)$$

The constraint equations ξ_1,ξ_2,ξ_3 and ξ_4 are used in this event:

$$\begin{aligned} \xi_1 &= \begin{bmatrix} x_h + l_1 \sin\alpha_1 - x_{a1} \\ y_h - l_1 \cos\alpha_1 \end{bmatrix} \\ \xi_2 &= \begin{bmatrix} x_h + l_2 \sin\alpha_2 - x_{a2} \\ y_h - l_2 \cos\alpha_2 \end{bmatrix} \\ \xi_3 &= [x_h + l_1 \sin\alpha_1 - x_{t1}]^2 + [y_h - l_1 \cos\alpha_1]^2 - l_{f11}^2 \\ \xi_4 &= [x_h + l_2 \sin\alpha_2 - x_{t2}]^2 + [y_h - l_2 \cos\alpha_2]^2 - l_{f21}^2 \end{aligned} \quad (2)$$

where x_{a1} and x_{a2} are the global x-coordinates of the latest foot strike (the x-coordinates of the ankles) of leg 1 and leg 2, while x_{t1} and x_{t2} are the global x-coordinates of the toes of leg 1 and leg 2. l_{f11} and l_{f21} are the distances between the ankle joint and the toe of leg 1 and leg 2. When the flat foot completely contacts the ground, the constraint equations ξ_1 and ξ_2 used to maintain foot contact with ground. ξ_3 and ξ_4 are used to constrain the ankle joint to move in the circular orbit mentioned above.

Matrix Σ_i transfers the independent generalized coordinates q into the constraint equation ξ_i, where $i = 1, 2, ..., 6$

$$\Sigma_i = \frac{d\xi_i}{dq} \quad (3)$$

Consequently, matrix Ψ_i is defined as follows:

$$\Psi_i = \frac{\partial(\Sigma_i \dot{q})}{\partial q}\dot{q} \quad (4)$$

Then we can obtain the Equation of Motion(EoM) in this state by the principle of virtual work (Suppose that leg 1 is

the stance leg while leg 2 is the swing leg):

$$\begin{bmatrix} M_r & \Sigma_1^T & \Sigma_4^T \\ \Sigma_1 & 0 & 0 \\ \Sigma_4 & 0 & 0 \end{bmatrix} \begin{bmatrix} \ddot{q} \\ F_1 \\ F_4 \end{bmatrix} = \begin{bmatrix} F_r \\ -\Psi_1 \\ -\Psi_4 \end{bmatrix} \tag{5}$$

where $\ddot{q}$ is the acceleration in the generalized coordinate. M_r is a reduced mass matrix:

$$[M_r] = [T]^T [M] [T] \tag{6}$$

Here matrix T, which can be described by $T = dq/dx$, transfers the independent generalized coordinates $\dot{q}$ into the velocities of the mass points $\dot{x}$. And F_r is the external force in generalized coordinates which is defined as follows:

$$\{F_r\} = [T]^T (\{F\} - [M] \{\ddot{x}\}) \tag{7}$$

Here F is the active external force. Note that the corresponding mass matrix in the rectangular coordinate M does not include the mass of the foot of swing leg as we described above. F_1 is the force acted on the ground by the stance leg, while F_4 is the force acted on the constraint circular orbit described by ξ_4. The specific analysis of the external force during ankle push-off can be found in our previous analysis [15]. When the knee joint releases the shank, the model moves to the shank releasing phase.

2) Shank releasing: Leg 1 (l_1) is still the stance leg, while leg 2 keeps swinging. In this phase (see Phase 2 in Fig. 2), the knee releases the shank, which is the only difference between Phase 2 and Phase 1. The constraint equations of the swing leg vary:

$$\begin{aligned} \tilde{\xi}_3 &= [x_h + (l_1 - l_{11}) \sin\alpha_1 + l_{11} \sin(\alpha_1 - \alpha_{11}) - x_{t1}]^2 \\ &+[y_h - (l_1 - l_{11}) \cos\alpha_1 - l_{11} \cos(\alpha_1 - \alpha_{11}))]^2 - l_{f11}^2 \\ \tilde{\xi}_4 &= [x_h + (l_2 - l_{12}) \sin\alpha_2 + l_{22} \sin(\alpha_2 - \alpha_{22}) - x_{t2}]^2 \\ &+[y_h - (l_2 - l_{22}) \cos\alpha_2 - l_{22} \cos(\alpha_2 - \alpha_{22}))]^2 - l_{f21}^2 \end{aligned} \tag{8}$$

$\tilde{\xi}_3$, $\tilde{\xi}_4$ are the same with ξ_3, ξ_4 when α_{11}, α_{22} are restricted to be zero. The constraint equations are still ξ_1 and ξ_2.

The EoM of the model in this event can be described by:

$$\begin{bmatrix} M_r & \Sigma_1^T & \Sigma_4^T \\ \Sigma_1 & 0 & 0 \\ \Sigma_4 & 0 & 0 \end{bmatrix} \begin{bmatrix} \ddot{q} \\ F_1 \\ F_4 \end{bmatrix} = \begin{bmatrix} F_r \\ -\Psi_1 \\ -\Psi_4 \end{bmatrix} \tag{9}$$

Note that the EoM is different from Equation (5). Here, since the knee is unlocked, the number of components of x and q increases. Phase 1 can be considered as a particular case of Phase 2. The time of shank swing can be adjusted to obtain a satisfied walking. When the direction of F_1 acting on the leg points to the toe, the swing leg is considered to leave the frictions constraint surface, which means the foot is out of contact with the ground. Then the leg swing phase starts.

3) Leg swing: In this phase (see Phase 3 in Fig. 2), leg 1 is the stance leg, while leg 2 swings freely and the shank is released. The springs on the compliant ankle of the swing leg constrains the foot vertical to the shank. The EoM of the model in this phase is:

$$\begin{bmatrix} M_r & \Sigma_1^T \\ \Sigma_1 & 0 \end{bmatrix} \begin{bmatrix} \ddot{q} \\ F_1 \end{bmatrix} = \begin{bmatrix} F_r \\ -\Psi_1 \end{bmatrix} \tag{10}$$

Note that the number of the components of M_r, q and f_r increases. Since leg 2 swings freely, f_c includes only T_1 in this phase. When the leg 2 has passed mid-stance and the shank swings to a relatively small angle, the knee is locked and the knee-strike occurs.

4) Knee-strike: This event starts when the knee is locked (see Phase 4 in Fig. 2). From the impact occurring due to knee-strike, we can have the following equations:

$$\begin{aligned} \overrightarrow{L_A^-} &= I_1\dot{\alpha}_1^-\vec{k} + \overrightarrow{AC} \times m_1\overrightarrow{v_{c1}^-} + I_{2t}\dot{\alpha}_2^-\vec{k} + \overrightarrow{AC_{2t}} \times m_{2t}\overrightarrow{v_{c2t}^-} \\ &+I_{2s}\dot{\alpha}_{22}^-\vec{k} + \overrightarrow{AC_{2s}} \times m_{2s}\overrightarrow{v_{2s}^-} + I_{2f}\dot{\alpha}_{22}^-\vec{k} + \overrightarrow{AC_{2f}} \times m_{2s}\overrightarrow{v_{2f}^-} \\ \overrightarrow{L_A^+} &= I_1\dot{\alpha}_1^+\vec{k} + \overrightarrow{AC} \times m_1\overrightarrow{v_{c1}^+} + I_2\dot{\alpha}_2^+\vec{k} + \overrightarrow{AC_2} \times m_2\overrightarrow{v_2^+} \\ &+I_{2f}\dot{\alpha}_2^+\vec{k} + \overrightarrow{AC_{2f}} \times m_{2s}\overrightarrow{v_{2f}^+} \\ \overrightarrow{L_H^-} &= I_{2t}\dot{\alpha}_2^-\vec{k} + \overrightarrow{HC_{2t}} \times m_{2t}\overrightarrow{v_{c2t}^-} + I_{2s}\dot{\alpha}_{22}^-\vec{k} \\ &+\overrightarrow{HC_{2s}} \times m_{2s}\overrightarrow{v_{c2s}^-} + I_{2f}\dot{\alpha}_{22}^-\vec{k} + \overrightarrow{HC_{2f}} \times m_{2f}\overrightarrow{v_{2f}^-} \\ \overrightarrow{L_H^+} &= I_2\dot{\alpha}_2^+\vec{k} + \overrightarrow{HC_2} \times m_2\overrightarrow{v_{c2}^+} + I_{2f}\dot{\alpha}_{22}^+\vec{k} \\ &+\overrightarrow{HC_{2f}} \times m_{2f}\overrightarrow{v_{2f}^+} \end{aligned} \tag{11}$$

with $\dot{\alpha}_1^-$ and $\dot{\alpha}_{22}^-$ the velocities before and $\dot{\alpha}_1^+$ and $\dot{\alpha}_2^+$ the velocities after the impact. $\vec{k}$ is the unit vector vertical to the motion plane. A is the contact point of the stance leg (ankle), while H is the point of the hip joint. C_1 and C_2 are the points of the CoM of the stance leg and the swing leg respectively. C_{2t} and C_{2s} are the points of the CoM of the thigh and the shank of the swing leg respectively. By the law of conservation of moment of momentum, we can obtain $\overrightarrow{L_A^-} = \overrightarrow{L_A^+}$ and $\overrightarrow{L_H^-} = \overrightarrow{L_H^+}$ from Equation (11) to calculate the velocities after the impact, $\dot{\alpha}_1^+$ and $\dot{\alpha}_2^+$.

Then leg 2 swings freely. The EoM of the model is still Equation (10) and f_c includes only T_1. If the heel contacts the ground, the heel-strike occurs.

5) Heel-strike: In this phase (see Phase 5 in Fig. 2), the heel contacts the ground (heel-strike occurs). The constraint equations in this phase are:

$$\begin{aligned} \xi_5 &= \begin{bmatrix} x_h + l_1 \sin\alpha_1 - l_{f12} \cos\alpha_1 - x_{he1} \\ y_h - l_1 \cos\alpha_1 - l_{f12} \sin\alpha_1 \end{bmatrix} \\ \xi_6 &= \begin{bmatrix} x_h + l_2 \sin\alpha_2 - l_{f22} \cos\alpha_2 - x_{he2} \\ y_h - l_2 \cos\alpha_2 - l_{f22} \sin\alpha_2 \end{bmatrix} \end{aligned} \tag{12}$$

where x_{he1} and x_{he2} are the x-coordinates of the heel of leg 1 and leg 2. The impact equation of the model changes to:

$$\begin{bmatrix} M_r & \Sigma_6^T \\ \Sigma_6 & 0 \end{bmatrix} \begin{bmatrix} \dot{q}^+ \\ F_6 \end{bmatrix} = \begin{bmatrix} M_r\dot{q}^- \\ -e\Sigma_6\dot{q}^- \end{bmatrix} \tag{13}$$

where $\Sigma_6 = \frac{d\xi_6}{dq}$, $\dot{q}^-$ and $\dot{q}^+$ are the velocities in the generalized coordinates before and after the heel-strike. And e is the collision coefficient. Since we assume the strike is a fully inelastic impact, e is zero in this model. F_6 is the force acting on the ground generated by the heel of leg 2. After the heel-strike, the foot of the swing leg pivots around the heel.

6) Heel pivot: In this phase (see Phase 6 in Fig. 2), the motion is similar to that in Phase 1. Leg 1(l_1) is still the stance leg, while leg 2 (l_2) is the swing leg. The knee joint is locked. The foot of leg 2 rotates around the ankle joint. The swing leg maintains heel contact with ground. The constraint equations ξ_7 and ξ_8 are used instead of ξ_3 and ξ_4 in this phase:

$$\xi_7 = [x_h + l_1 \sin\alpha_1 - x_{he1}]^2 + [y_h - l_1 \cos\alpha_1]^2 - l_{f12}^2$$
$$\xi_8 = [x_h + l_2 \sin\alpha_2 - x_{he2}]^2 + [y_h - l_2 \cos\alpha_2]^2 - l_{f22}^2 \quad (14)$$

where x_{he1} and x_{he2} are the global x-coordinates of the heels of leg 1 and leg 2. l_{f12} and l_{f22} are the distances between the ankle joint and the heel of leg 1 and leg 2. ξ_7 and ξ_8 are used to constrain the ankle joint to move in the circular orbit mentioned above in this phase.

The EoM of the model in this state is:

$$\begin{bmatrix} M_r & \Sigma_1^T & \Sigma_8^T \\ \Sigma_1 & 0 & 0 \\ \Sigma_8 & 0 & 0 \end{bmatrix} \begin{bmatrix} \ddot{q} \\ F_1 \\ F_8 \end{bmatrix} = \begin{bmatrix} F_r \\ -\Psi_1 \\ -\Psi_8 \end{bmatrix} \quad (15)$$

The corresponding mass matrix in the rectangular coordinate M does not include the mass of the foot of swing leg as we described above. F_8 is the force acting on the constraint circular orbit described by ξ_8. And F_r is still the external force in generalized coordinates obtained by Equation (7). When the ankle joint contacts the ground, the toe-strike occurs.

7) Toe-strike: In this phase (see Phase 7 in Fig. 2), the whole foot of the swing leg has an impact with the ground. The impact equation of the model is:

$$\begin{bmatrix} M_r & \Sigma_2^T \\ \Sigma_2 & 0 \end{bmatrix} \begin{bmatrix} \dot{q}^+ \\ \tilde{F}_2 \end{bmatrix} = \begin{bmatrix} M_r\dot{q}^- \\ -e\Sigma_2\dot{q}^- \end{bmatrix} \quad (16)$$

where $\Sigma_2 = \frac{d\xi_2}{dq}$, $\dot{q}^-$ and $\dot{q}^+$ are the velocities in the generalized coordinates before and after the heel-strike. The collision coefficient e is still zero. $\tilde{F}_2$ is the force acting on the ground generated by the whole foot of leg 2. After the foot-strike, the model moves back to Phase 1. The stance leg and the swing leg will exchange the role in the next step.

In each phase as mentioned above, falling down and running are are constantly monitored throughout the simulated walking. In Phase 4, shank releasing is detected and serious foot-scuffing is detected in both Phase 3 and Phase 4. If these cases happen, the walker will be restricted to stop.

C. Dynamic stability

For a stable dynamic walker which is a purely periodic limit cycle system, local stability is defined from Floquet theory [12], which describes how limit cycle systems respond to local perturbations from one cycle to the next. In this study, similar to the previous model [16], the stability was quantified by the modulus of the Jacobian matrix of the mapping function. The points in the phase-space graph that map onto themselves after a step called fixed points, which represent a continuous stable walking motion. If a small deviation away from the initial conditions of a fixed point disappears over a number of steps until the walker is back in its limit cycle, the fixed point is stable and a stable continuous walking is found. Assume that the mapping of the points is presented by the equation:

$$v_{n+1} = f(v_n) \quad (17)$$
$$v_{n+1} = v_s + \Delta v_{n+1} \quad (18)$$
$$v_n = v_s + \Delta v_n \quad (19)$$

where v_s is a fixed point, and f is a short notation for the complete simulation of one walking step including the foot strike impacts (foot-strike of point-foot walker and round foot walker, heel-strike and toe-strike of flat-foot walker). By linearized analysis, the relation of the small deviations from Δv_{n+1} and from Δv_n can be simplified to:

$$\Delta v_{n+1} = J\Delta v_n \quad (20)$$

where J is the Jacobian matrix $\frac{\partial f}{\partial V}$. If all the eigenvalues of J have a modulus smaller than 1, the deviations decrease step after step and the walking motion is stable, the fixed point v_s can be called a stable fixed point. Moreover, as mentioned in the previous model [16], a fixed point can be found by a Newton-Raphson iteration as repeating the procedure as the following:

$$\Delta v = |I - J|^{-1}(f(v) - v) \quad (21)$$
$$v = v + \Delta v \quad (22)$$

until $|\Delta v| < \varepsilon$. Here ε is a very small positive number related to the accuracy allowed.

The mapping function f and the Jacobian matrix J are different for different sets of parameters. Notate the maximal eigenvalue as λ_m, which represents the decreasing speed of the deviation. Since the corresponding λ_m may be different, the stability grades may be different for different sets of parameters even they all have a stable fixed point. The smaller $\mid \lambda_m \mid$ is, the faster the deviation decreases, the more stable the walker is. The similar conclusion can be obtained when all sets of parameters only have an unstable fixed point. The larger the $\mid \lambda_m \mid$ is, the more far from the stable state the walker is.

Evaluation of the walking motion on an irregular surface is another method to measure the dynamic stability of bipedal locomotion. In this study, we examined whether the walker can manage without falling over as the irregularity of the walking surface was increased from zero (i.e., a smooth continuous slope) up to the maximum level. Specifically in the evaluation, the biped walks on the ground with a step down (denoted as h), which describe the irregularity of the slope. Note that, the slope angle does not vary in the walking path. The irregularity h increases until the walker can not manage. Then the maximal allowable h, notated as h_m, reveals the ability of handling global disturbance. The bigger the h_m, the more stable the walker is.

III. Results

In this study, all distances and point masses are normalized by leg length and whole body mass respectively. All simulations and data processing were performed using Matlab 7 (The Mathworks, Inc., Natick, MA).

A. Walking simulations

In the simulations, the biped is restricted to stop in three cases, including falling down, running and shank releasing. We consider that the walker falls down if the angle of either leg exceeds the normal range. And the model is running when all the forces act upwards on the walker provided by the floor. Shank releasing which means the shank of the swing leg is not locked before "heel-strike". Foot-scuffing, which often appears when the the knee joint locks the shank too early, is another case that the walker maybe have to stop. It is likely avoided for a real three-dimensional walker with lateral motion, thus we allow this to happen if the foot travels below the floor not very seriously.

The walker detects current conditions to decide knee-locking and knee-unlocking actions. During the leg swing phase, since the existence of the passive knee joints, the shank swings freely. In our simulations, if the relative angle between the shank and the thigh decreases to a certain value, e.g. 0.1rad and keeps decreasing, the knee joint will lock and keep the thigh and the shank of the swing leg in a straight line. The knee unlocking event is slightly different to other existing studies of walking simulation. In our study, if the foot of the swing leg fully contacts the ground (toe-strike occurs), the knee of the stance leg will not unlock immediately. After a very short while (preset time, e.g. $0.02s$), the knee of the swing leg unlocks and releases the shank to swing freely. The reason of having this difference is to make the ankle spring of the stance leg act fully during the foot lifting. Then the result of the walking simulation is more close to real human walking.

In the simulations, the proposed six-link model takes a stable bipedal waking step which shows a resemblance to the human gait (see Fig. 3). Since be more close to human

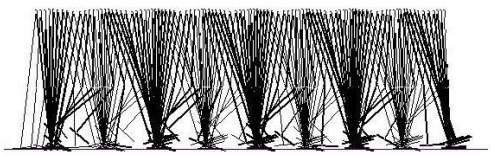

Fig. 3. Stick diagram of dynamic bipedal walking obtained from the simulations. The procedure of the simulation is a succession of nonlinear numerical dynamic simulations of walking steps which begin and end at the instant immediately after foot strike. Within one step, the EoMs are numerically integrated until one of the seven events is detected.

characteristics, our model solved the typical non-human aspects of the existing models [6], [16]. First, the feet in the proposed model are flat, hence the heel-strike and toe-strike impulses, which are important in human walking gaits [13], [9], can be analyzed. In addition, the ankle stiffness simulates the tendons and muscles of human beings during walking. Moreover, the knee joints of the model can prevent from foot-scuffing when the swing leg passes the mid-stance.

The step starts and ends immediately after a toe-strike as described in Fig. 2. The hip torque actuates the pelvis to move forward like an inverted pendulum with controllable speed, while the swing leg swings to a forward position.

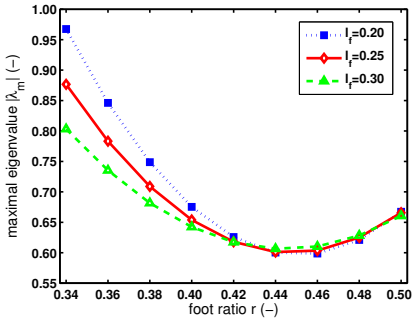

Fig. 5. Effects of foot ratio on local stability of dynamic bipedal walking.

When the heel contacts the ground, the foot will rotate around the heel until the toe-strike impulse occurs. Fig. 4 shows the trajectories of the different parts of the model.

B. Effects of foot ratio

Using the simulations, we investigated the effects of varying the foot length l_f and foot ratio r on walking stability. Fig. 5 shows the maximal eigenvalue λ_m of the Jacobian matrix (indicates dynamic stability) of the biped when varying the foot geometric parameters. Since the smaller the λ_m is, the faster the deviation decreases, the more stable the walker is, from Fig. 5, it seems that there exists an optimal foot ratio in view of dynamic stability. For example, when foot length $l_f = 0.2$ (see the dotted line in Fig. 5), if $r < 0.4$, the maximal eigenvalue λ_m decreases rapidly as r increases. It indicates that there is an optimal r with the smallest λ_m. The optimal foot ratio exists in the range from 0.44 to 0.46, where the foot length is in the range from 0.2 to 0.3. Such optimal foot-ankle ratio is close to the human data [1], [2], approximately 0.4 in the human foot.

In addition, we evaluated the maximal allowable ground disturbance h_m when varying the foot length l_f and foot ratio r. Fig. 6 shows the results. It is clear that as the foot length increased (within a certain range), the walker can handle larger ground disturbance. Furthermore, for a fixed foot length, it seems that there is an optimal foot-ankle ratio to obtain largest h_m. For example, when foot length is 0.2, as the foot-ankle ratio increased, the walker obtains the largest h_m when foot-ankle ratio is about 0.4 (see the dash line in Fig. 6). Such optimal foot-ankle ratio is also close to that of human foot, approximately 0.4. However, to obtain largest h_m, the optimal foot-ankle ratio increases to 0.5 (see the solid line in Fig. 6).

IV. Discussion

Adding flat feet and passive ankle stiffness to dynamic bipedal walking model show a remarkable resemblance to the human gait. The proposed six-link dynamic walking model that takes heel-strike and toe-strike into account is more close to real human walking than the existing models that take no effects of foot shape into account [6], [5], [16]. Since the modeling methods, there were several limitations of the point-foot models [6], [5], [16] and the flat-foot models with

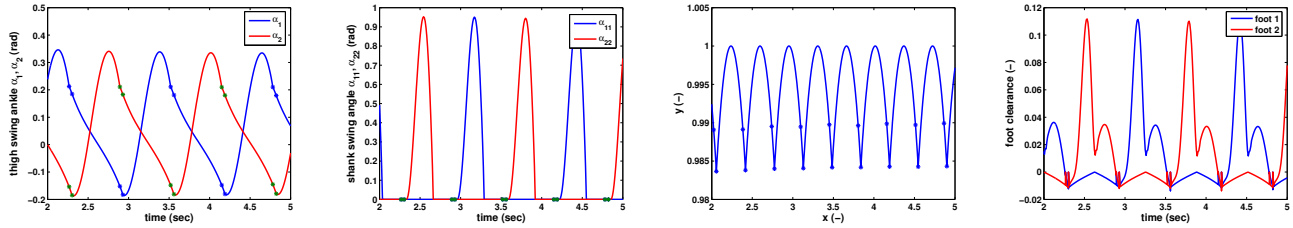

(a) (b) (c) (d)

Fig. 4. Trajectories of different parts of the model during simulated walking. (a) shows the absolute angles of the stance thigh and swing thigh, while (b) shows the absolute angles of the stance shank and swing shank. (c) indicate the trajectory of the hip joint in global coordinates during walking. (d) shows the change of the foot clearance (the vertical distance between the lowest point of each foot and the level ground.)

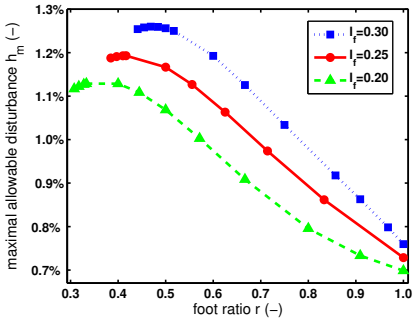

Fig. 6. Effects of foot ratio on global stability of dynamic bipedal walking.

no ankles [9]. These two types of adapted simplest walking models emulate several key characteristics of human walking. For example, since these models employed instantaneous step transitions, there is no double support phase.

Since the proposed flat-foot model with compliant ankles has the capability to sustain a double stance phase, the optimal foot shape (foot length and foot ratio) is close to that of humans. Former studies on optimal foot shape for bipedal walking mainly focus on the energetic efficiency [13], [9]. From the view of efficiency, optimal foot ratio is greater than 0.5 [9] (different from the definition of foot-ankle ratio in our study, equal to $r = 1$ if converts to our definition), which is far from the human foot shape. There are several aspects that result in such differences. First, the inexistence of double stance phase affects the stability of the walker. Another possibility is the lack of the degree of complexity in ankle, comparing with the human foot. Thus, the results of analyzing effects of foot ratio on dynamic stability of the flat-foot model with compliant ankles is more reliable and explores further understanding of the human foot shape and its significance. The optimal foot ratio of such model is in the range from 0.44 to 0.46. For the foot length in range from 0.2 to 0.3, the simulation results indicate that relatively small foot ratio results in lower local stability and adaptability to terrain disturbance. It further suggests that the proportion of the human foot is to some extent the product of positive selection for more stable bipedal walking during evolution of the foot ($r = 0.282$ in chimpanzees and $r = 0.196$ in orangutans [2]).

There are several differences between the presenting modeling results and human walking. First, optimal foot ratio is still larger than that of the human foot. In addition, the largest perturbation that the walker can handle is far from the human performance. More bio-mimetic models that may be interesting to explore include a walker with toe joints to obtain more anthropomorphic toe-strike and toe-off impulse. The addition of some sort of ankle or toe actuation would also be useful to study.

REFERENCES

[1] A. H. Schultz, The relative lengths of the foot skeleton and its main parts in primates, Symposia of the Zoological Society of London **1**:199–206, 1963.

[2] L. Aiello, C. Dean, An introduction to human evolutionary anatomy, Academic Press, London, 507–538. 1990.

[3] W. J. Wang, R. H. Crompton, Analysis of the human and ape foot during bipedal standing with implications for the evolution of the foot, Journal of Biomechanics **37**:1831–1836, 2004.

[4] E. Borzova, Y. Hurmuzlu, Passively walking five-link robot, *Automatica* **40**:621–629, 2004.

[5] A. Goswami, B. Espiau, B.A. Thuilot, A study of passive gait of a compass-like biped robot: symmetry and chaos, *International Journal of Robotics Research* **17**:1282–1301, 1998.

[6] M. Garcia, A. Chatterjee, A. Ruina, M. Coleman, The simplest walking model: stability, complexity, and scaling, *Journal of Biomechanical Engineering* **120**:281–288, 1998.

[7] Y. Hurmuzlu, C. Basdogan, On the measurement of dynamic stability of human locomotion, *Journal of Biomechanical Engineering* **116**:30–36, 1994.

[8] A. D. Kuo, Energetics of actively powered locomotion using the simplest walking model, *Journal of Biomechanical Engineering* **124**:113–120, 2002.

[9] M. Kwan, M. Hubbard, Optimal foot shape for a passive dynamic biped, *Journal of Theoretical Biology* **248**:331-339, 2007.

[10] T. McGeer, Passive dynamic walking, *International Journal of Robotics Research* **9**:68–82, 1990.

[11] S. Mochon, T. McMahon, Ballistic walking, *Journal of Biomechanics*, **13**:49–57, 1980.

[12] A. H. Nayfeh, B. Balachandran, *Applied Nonlinear Dynamics: Analytical, Computational, and Experimental Methods*, John Wiley & Sons, New York, 1995.

[13] A. Ruina, J. E. A. Bertram, M. Srinivasan, A collisional model of the energetic cost of support work qualitatively explains leg sequencing in walking and galloping, pseudo-elastic leg behavior in running and the walk-to-run transition, *Journal of Theoretical Biology* **237(2)**:170–192, 2005.

[14] A. Ruina, Passive-dynamic locomotion, Fifth World Congress of Biomechanics Conference, *Journal of Biomechanics* **39(SI)**:S359, 2006.

[15] Q. Wang, Y. Huang, L. Wang, Passive dynamic walking with flat feet and ankle compliance, *Robotica*, **28**(3): 413–425, 2010.

[16] M. Wisse, A. L. Schwab, F. C. T. van der Helm, Passive dynamic walking model with upper body, *Robotica* **22**:681–688, 2004.